2010-01-01

Visible Near-Infrared Hyperspectral Imaging for the Identification and Discrimination of Brown Blotch Disease on Mushroom (Agaricus bisporus) Caps

Edurne Gaston
Dublin Institute of Technology, edurne.gaston@student.dit.ie

Jesus Maria Frias
Dublin Institute of Technology, Jesus.Frias@dit.ie

Patrick J. Cullen
Dublin Institute of Technology, pjcullen@dit.ie

Colm O'Donnell
University College Dublin

Aoife Gowen
University College Dublin, aoife.gowen@ucd.ie

Follow this and additional works at: http://arrow.dit.ie/schfsehart

Part of the Agriculture Commons, and the Food Processing Commons

1 Visible Near-Infrared Hyperspectral Imaging for the Identification and

2 Discrimination of Brown Blotch Disease on Mushroom (*Agaricus bisporus*)

3 Caps

EDURNE GASTON[1], JESÚS M. FRÍAS[1*], PATRICK J. CULLEN[1], COLM P. O'DONNELL[2] and AOIFE A. GOWEN[2].

[1]School of Food Science and Environmental Health, Dublin Institute of Technology, Cathal Brugha Street, Dublin 1, Ireland.

[2]Biosystems Engineering, School of Agriculture, Food Science and Veterinary Medicine, University College Dublin, Dublin 4, Ireland.

*Corresponding author. E-mail: Jesus.Frias@dit.ie

Abstract

Brown blotch, caused by pathogenic *Pseudomonas tolaasii* (*P. tolaasii*), is the most problematic bacterial disease in *Agaricus bisporus* mushrooms. Although it does not cause any health problems, it reduces the consumer appeal of mushrooms in the market place, generating important economical losses worldwide. Hyperspectral imaging (HSI) is a non-destructive technique that combines imaging and spectroscopy to obtain information from a sample. The objective of this study was to investigate the use of HSI for brown blotch identification and discrimination from mechanical damage on mushrooms. Hyperspectral images of mushrooms subjected to i) no treatment, ii) mechanical damage or iii) microbiological spoilage were taken during storage and spectra representing each of the classes were selected. Partial least squares- discriminant analysis (PLS-DA) was carried out in two steps: i) discrimination between undamaged and damaged mushrooms and ii) discrimination between damage sources (i.e. mechanical or microbiological). The models were applied at a pixel level and a decision tree was used to classify mushrooms into one of the aforementioned classes. A correct classification of >95% was achieved. Results from this study could be used for the development of a sensor to detect and classify mushroom damage of mechanical and microbial origin, which would facilitate the industry to make rapid and automated decisions to discard produce of poor marketability.

Keywords: mushrooms, *Agaricus bisporus*, brown blotch, *Pseudomonas tolaasii*, mechanical damage, vis-NIR hyperspectral imaging, PLS-DA.

Introduction

Cultivated mushrooms are susceptible to a variety of pests and diseases. *Pseudomonas tolaasii* (*P. tolaasii*) is the causal agent of brown blotch (also known as bacterial blotch) disease[1] and the most important pathogenic bacterium of *Agaricus bisporus*[2]. This disease has been detected and described worldwide and affects not only the button mushroom market but the mushroom market in general[3]. According to growers, brown blotch is "the worst disease", because of the large economic losses associated to it. Brown blotch can cause a general loss of crop yield of 10 % and a decrease in quality of another 10 %[4]. The most typical symptoms of brown blotch are pitting and browning of mushroom tissues, induced by the watersoluble toxin tolaasin[5]. This extracellular toxin is produced by the pathogenic form of *P. tolaasii*[6]. The colonisation of mushroom caps by *P. tolaasii* results in the appearance of unappealing brown spots on the mushroom cap and stipe[3]. Lesions are slightly concave blemishes, sometimes small, round or spreading in many directions[7]. When the damage is more intense, the spots are darker and sunken. Browning affects only the external layers of the cap tissue and is restricted to 2-3 mm below the surface of the cap.

The mushroom industry is in need of objective evaluation methodologies to ensure that only high quality produce reaches the market[8]. Studies in the field of brown blotch detection include the work of Vízhányó and Felföldi[9], who tested the potential of a machine vision system to recognise and identify brown blotch and ginger blotch diseases, both of which cause discolouration in mushroom caps. A vectorial normalisation method was developed to decrease the effect of the natural loss of whiteness of the mushroom surface and increase the differences in the image caused by the disease. The method showed an ability to discriminate between discolouration caused by microbial disease and other sources of discolouration, such as natural senescence. However, no attempt was made to discriminate brown blotch from

49 bruises induced by mechanical stress, which is also an important source of discolouration and

50 quality loss in the mushroom industry[10].

51 Hyperspectral imaging (HSI) is a rapid and non-destructive technology that has recently

52 emerged as a powerful alternative to conventional imaging for food analysis[11]. Hyperspectral

53 images are composed of hundreds of contiguous wavebands for each spatial position of an

54 object. Consequently, each pixel in a hyperspectral image contains the spectrum of that

55 specific position. Hyperspectral images, known as *hypercubes*, are three-dimensional blocks

56 of data, comprising two spatial and one wavelength dimension. The large quantities of highly

57 correlated data contained in a hypercube are well suited to analysis by dimension reduction

58 approaches such as principal components analysis (PCA) and partial least squares-

59 discriminant analysis (PLS-DA)[12]. PLS-DA can also be applied to develop qualitative models

60 for supervised classification between various sample classes.

61 HSI has been applied at various levels in the assessment of safety and quality of food,

62 including constituent analysis[13-15], quality evaluation[16, 17] and detection of contaminants[18, 19]

63 and defects[20]. Additionally, a number of researchers have reported the potential of HSI for

64 identification of microorganisms of concern in food[21, 22]. In the field of mushrooms, HSI has

65 proved useful for the detection of bruise[23] and freeze[24] damage and the prediction of moisture

66 content[25] and enzyme activity[26], as well as for the evaluation of shelf-life[27] and quality

67 deterioration[28]. Recent advances in the detection of skin damage of other products include

68 work by Ariana et al.[29] with cucumbers and Nicolaï et al.[30] and ElMasry et al.[31] with apples.

69 As regards damage of microbial origin, Gómez-Sanchis et al.[32] proposed a hyperspectral

70 imaging system for the early detection of rot caused by *Penicillium digitatum* (fungi) in

71 mandarins. This method's success in classifying rotten fruit was above 91% and it

72 represented an alternative to the operationally inefficient sorting system previously used in

73 the citrus industry. While evidence from the literature points to its feasibility, to the authors'

4

74 knowledge, HSI has not been used to detect damage of bacterial origin in horticultural
75 products.

76 The objective of this study was to investigate the potential application of Vis-NIR HSI for
77 brown blotch identification on mushroom caps and for its discrimination from mechanical
78 damage injuries.

79

Materials and methods

Mushroom supply and damage

82 *Agaricus bisporus* mushrooms (strain Sylvan A15, Sylvan Spawn Ltd., Peterbourough, UK)
83 were grown in plastic bags and tunnels in Kinsealy Teagasc Research Centre (Kinsealy, Co.
84 Dublin, Ireland) following common practice in the mushroom industry. Only uniform
85 undamaged closed cap mushrooms from the 1st and 2nd flush with a diameter of 3-5 cm were
86 hand-picked in November 2008 (training set) and July 2009 (test set). Samples were placed in
87 a metal grid and carefully delivered to the laboratory in purpose-built containers, to minimise
88 mechanical damage during transport**.** Mushrooms arrived at the laboratory premises within 1
89 hour after harvesting and were stored overnight at 4°C.

90 For each set of mushrooms (n_{train} = 144 and n_{test} = 108), samples were divided in 3 groups
91 (undamaged (U), mechanically damaged (MD) and *P. tolaasii* inoculated mushroom (PT)) of
92 equal size ($n_{train,i}$ = 48 and $n_{test,i}$ = 36, where i = U, MD, PT).

93 Each mushroom class was treated as follows:

94   U: No treatment.

95   MD: samples were subjected to vibrational bruising to simulate crop handling and
96 transport. Mushrooms were damaged in batches of 600g (approx) units inside polystyrene
97 plastic boxes. Mechanical damage was induced by using a Gyratory Shaker Model G2

98   shaking table (New Brunswick scientific Co., Edison, N.J., USA) at 300 rpm amplitude for a

99   shaking period of 10 min. Samples were stored in an environmental incubator (MLR-350 HT,

100 SANYO Electric Biomedical Co. Ltd., Japan) at 25°C and 90 % relative humidity (RH) for

101 24 h prior to imaging.

102   PT: samples were obtained by inoculating 4 drops of 10 µL/each of a solution of

103 pathogenic *P. tolaasii* onto each clean cap at 4×10^6 cfu. Samples were stored in the

104 incubator for 48 h at 25°C and 90 % RH prior to imaging, to encourage appearance of brown

105 blotch symptoms on the mushroom caps.

106 A total number of 252 mushrooms were used in this experiment.

107 <u>Pathogenic *P. tolaasii* solution</u>

108 Freeze-dried culture (DMS no. 19342) was purchased from Deutsche Sammlung von

109 Mikroorganismen und Zellkulturen GmbH (DSMZ), Germany, resuspended in nutrient broth

110 (NB, Scharlau, Dublin) and incubated at 25°C for 24 h. The pure culture was transferred into

111 nutrient agar plates (NA, Oxoid, Dublin) and incubated at optimal conditions to obtain

112 isolated colonies.

113 "Mushroom tissue block rapid pitting" and "White Line in Agar" (WLA) pathogenicity tests

114 were carried out following the procedure of Wong and Preece[33] to confirm culture

115 pathogenicity on mushrooms.

116   -   *Mushroom tissue block rapid pitting test*

117 The outer skin of a mushroom was peeled off and mushroom cap tissue blocks of approx.

118 $15 \times 15 \times 5$ mm were cut. Bacterial isolates were grown on Pseudomonas agar base

119 (PAB, Oxoid, Dublin) at 25°C for 24 h and suspended in sterile distilled water (10^8 cfu

120 mL^{-1} approx). Mushroom blocks were placed in duplicate on Petri dishes containing

121 sterile water-moistened filter paper. The bacterial solution was inoculated onto the cut

122   surface of one of the mushroom blocks and incubated at 25°C. Sterile water was

123   inoculated onto the surface of the other mushroom blocks for negative control. Pitting of

124   the cut surface of mushroom tissue revealed pathogenicity of *P. tolaasii* on the mushroom

125   blocks.

126   *"White Line in Agar" test*

127   *Pseudomonas reactans* (*P. reactans*) was streaked out in a line, directly from agar slope

128   culture, across PAB in a Petri dish. This strain had been isolated and provided by

129   Kinsealy Teagasc Research Centre.

130   The *P. tolaasii* isolate to be tested was streaked immediately after on to the plates at right

131   angles to the reacting organism (i.e. *P. reactans*). Plates were incubated at 25°C for 24 h

132   for the production of a white line with the reacting organism.

133   White line production in the agar between *P. reactans* and *P. tolaasii* was interpreted as

134   positive interaction between colonies and a positive response for pathogenicity test.

135   A loopfull of pathogenicity confirmed working culture was transferred to a sterile 0.8% saline

136   solution (Sigma, Dublin). 4 droplets of 10 μL/each of a 10^8 cfu mL^{-1} solution were inoculated

137   onto the cap, resulting in inoculation concentration of 4×10^6 cfu.

138   **Hyperspectral imaging**

139   Hyperspectral images were obtained using a pushbroom line-scanning HSI instrument (DV

140   Optics Ltd, Padua, Italy). The instrument comprised a moving table, illumination source (150

141   W halogen lamp source attached to a fibre optic line light positioned parallel to the moving

142   table), mirror, objective lens (25 mm focal length), Specim V10E spectrograph (Spectral

143   Imaging Ltd, Oulu, Finland) operating in the wavelength range of 400-1000 nm

144   (spectroscopic resolution of 5 nm), CCD camera (Basler A312f, effective resolution of 580 ×

145   580 pixels by 12 bits), acquisition software (SpectralScanner, DV Optics, Padua, Italy) and

146 PC. A cylindrical diffuser was placed in front of the fibre optic line light to produce a diffuse

147 light source. In this study, only spectral data within the wavelength range of 445-945 nm

148 were used, as beyond this range the noise level of the camera was high and the signal

149 efficiency of the light source was low.

150 Reflectance calibration

151 Reflectance calibration was carried out prior to mushroom image acquisition in order to

152 account for the background spectral response of the instrument and the "dark" camera

153 response. The bright response ("*W*") was obtained by collecting a hypercube from a uniform

154 white ceramic tile; the dark response ("*dark*") was acquired by turning off the light source,

155 completely covering the lens with its cap and recording the camera response. The corrected

156 reflectance value ("*R*") was calculated from the measured signal ("*I*") on a pixel-by-pixel

157 basis as shown by:

158
$$R_i = \frac{(I_i - dark_i)}{(W_i - dark_i)}$$

159 where i is the pixel index, i.e. i=1,2,3,…,n and n is the total number of pixels.

160 HSI images of U mushrooms were acquired on day 0 of the experiment. MD mushrooms

161 were scanned after 24 h of storage. PT mushroom images were taken after 48 h of storage.

162 Data were recorded in units of reflectance and saved in ENVI header format using the

163 acquisition software.

164 **Confirmation of *P. tolaasii***

165 After image acquisition of PT mushrooms on day 2 of storage, 0.5 g of the outer skin of 10 %

166 of each mushroom class were extracted with a sharp sterile knife. Skins were suspended

167 separately in 10 mL of a 0.8 % saline solution. Samples were homogenised in a stomacher

168 (Seward BA 7020, Seward, UK) for 60 s at high intensity. Serial dilutions of each suspension

169 were prepared and transferred onto NA and PAB plates, which were incubated for 48 h at

170 25°C to obtain isolated colonies. The same procedure had been carried out after image

171 acquisition of U mushrooms on day 0 and resulting colonies were used as negative controls.

172 Serial dilutions of the pathogenic *P. tolaasii* solution that had been used to inoculate PT

173 mushrooms were also prepared and transferred onto NA and PAB plates; resulting colonies

174 were used as positive controls.

175 Mushroom tissue block rapid pitting and WLA tests were carried out to test for pathogenicity

176 of isolated colonies.

177 **Image processing**

178 For each mushroom hyperspectral image, 175 characteristic (i.e. U, MD or PT, depending on

179 mushroom class) regions of interest (ROI) were selected by using an interactive selection tool

180 ("*ROI tool*") available in the acquisition software. The ROI's were 3×3 pixels in size and

181 were selected from the central region of the mushroom cap, where possible. Selecting spectra

182 from analogous surface areas in all the mushrooms aimed at minimising the scaling

183 differences caused by mushroom surface curvature[24]. The average reflectance spectrum ("*R*")

184 of each ROI was obtained by averaging the pixel spectra of the region. Spectral data of each

185 mushroom set were used to build two-dimensional matrices, where each row represented the

186 spectrum of one ROI.

187 Prior to the development of multivariate models for damage class prediction, spectra were

188 pre-processed using the Standard Normal Variate (SNV) transformation to reduce spectral

189 variability due to non-chemical biases[34].

190 Training set matrices (raw and SNV-corrected) contained 8400 spectra and test set matrices

191 (raw and SNV) contained 6300 spectra.

Partial least squares- discriminant analysis (PLS-DA)

Partial least-squares discriminant analysis was applied to the training set matrices (raw and SNV-corrected, n=8400) using MATLAB 7.0 (The Math Works, Inc. USA). The aim was to build models that would enable maximum separation of sample spectra into different classes depending on their physical condition. A two step model approach was taken for each set of spectra (i.e. raw and SNV): one model (namely "U/Dam" model) was developed to discriminate between undamaged (U) and damaged (Dam) spectra and another model (namely "MD/PT" model) was built to discriminate between the two classes of Dam, i.e. mechanical (MD) and microbiological (PT). Overall, four models were built: U/Dam_raw, U/Dam_SNV, MD/PT_raw and MD/PT_SNV.

For this purpose, a dummy response variable, Y, was constructed and assigned to each spectrum. For U/Dam models, $Y = 0$ for U spectra and $Y = 1$ for Dam spectra. For MD/PT models, $Y = 0$ for MD spectra and $Y = 1$ for PT spectra. In both cases, a cut-off value of 0.5 was used to classify spectra, as suggested by Esquerre, Gowen, O'Donnell & Downey[35]; spectra with a predicted dummy variable <0.5 were identified as belonging to class 0, while those with predicted Y-value ≥0.5 were classified as belonging to class 1.

Spectra from the training data set were split into 10 sections and continuous blocks cross-validation was performed. The decision on the number of latent variables (# LV) to select for each model was made based on the root-mean square error of cross-validation (RMSECV), which is the mean of the sum of squared differences between the actual and the predicted value of the dummy variable.

The models were also applied to the test set matrices (raw and SNV-corrected, n=6300), which represented independent sets of sample spectra. Performance of the classification models was evaluated on the basis of their sensitivity (number of spectra of a given type

216   correctly classified as that type) and specificity (number of spectra not of a given type

217   correctly classified as not of that type) on training and test sets.

218   **Prediction maps**

219   An important feature of hyperspectral imaging is the ability to map the distribution of

220   components/attributes on samples. In this case, developed PLS-DA models could be applied

221   to entire hypercubes of mushrooms to form two dimensional prediction images where the

222   damage class of each pixel as predicted by the PLS-DA models would be represented by its

223   intensity ("I"). With this in mind, the following step-by-step procedure was carried out on all

224   mushroom hypercubes:

225   1. Masking. This step was performed to separate the mushroom pixels from the

226   background. The mask was created by thresholding the mushroom image at 940 nm,

227   where a pixel threshold value of 0.1 was used to segment the mushroom from the

228   background. All background regions were set to zero and only the non-zero elements

229   of the image were used in further steps.

230   2. Erosion. As all the spectra collected to build the models corresponded to interactively

231   selected ROI's of the central part of the mushrooms, the image outline (i.e. edge) of

232   the mushrooms was eroded to spectra showing differences due to sample curvature.

233   This was done by eroding the masks using disk-shaped structuring elements (SE,

234   whose radii increased from 0 –i.e. no erosion- to 40 pixels, in 10 pixel gaps), prior to

235   the application of PLS-DA models. The effect that varying the radius of the SE had on

236   i) the area of the mask, ii) the pixel distribution of the predicted maps and iii) the

237   performance statistics of the two models at a pixel level, based upon ANOVA results

238   obtained using R[36], was studied.

239   3. <u>Application of developed PLS-DA models</u>. The U/Dam model was applied to eroded
240   hypercubes and following this classification, the MD/PT model was applied only to
241   the pixels previously classified as *Dam*. Three binary images (Bin$_U$, Bin$_{MD}$ and Bin$_{PT}$,
242   one for each damage class, where 1 indicated class membership and 0 indicated non-
243   membership) were generated after classifying each pixel as "*U*" ($I_{U/Dam}<0.5$), "*MD*"
244   ($I_{U/Dam}>0.5$ and $I_{MD/PT}<0.5$) or "*PT*" ($I_{U/PT}>0.5$ and $I_{MD/PT}>0.5$) tissue.

245   4. <u>Closing</u>. As enzymatic browning was expected to develop uniformly across MD
246   mushroom caps and bacterial lesions were expected to appear as brown spots of
247   visible size, Bin$_{MD}$ images *closed*[37] in order to avoid noise in the form of isolated *PT*
248   pixels in such maps. The *Closing* morphological operator performs dilation followed
249   by erosion; this was done using a diamond-shaped SE with a radius of 3 pixels. The
250   effect of omitting/incorporating Step 4 on i) the pixel distribution of the prediction
251   maps and ii) performance statistics, based upon ANOVA results, was investigated.

252   5. <u>Concatenation</u>: the three binary maps (i.e. Bin$_U$, Bin$_{MD}$ and Bin$_{PT}$) were concatenated
253   to build false colour maps where *U*, *MD* and *PT* classified pixels were represented in
254   green, red and blue, respectively.

Mushroom classification

256 Based on the percentage of pixels of each damage class on the prediction map, a decision tree

257 (shown in Figure 1) was used to allocate each mushroom to one of the three mushroom

258 classes. As the main objective of this work was to identify *P. tolaasii* inoculated mushrooms,

259 the *PT* pixel percentage of the prediction maps was selected as the discrimination criteria and

260 a cut-off value was established by exploring the pixel histograms of the Bin$_{PT}$ images of U,

261 MD and PT mushrooms (Figure 2). A *PT* pixel percentage of 2 % appeared to be a reasonable

262 cut-off point, as all of the U mushroom predictions and almost all of the MD mushroom

263 predictions exhibited lower values and almost all of the PT mushroom predictions showed

264 higher values. After visual inspection of the two PT mushrooms that were below the cut-off

265 value, it was observed that these two mushrooms did not develop any brown blotch on their

266 caps, for which they could be left out for cut-off establishment purposes. As it can be seen in

267 the figure, when the number of *PT* pixels in the prediction image was higher than 2 %, the

268 mushroom was classified as PT. If the number of *PT* pixels was lower than 2 % and the

269 amount of *MD* pixels was higher than the amount of *U* pixels, the mushroom was classified

270 as MD. Finally, if the number of *PT* pixels was lower than 2 % and the amount of *MD* pixels

271 was lower than the amount of *U* pixels, the mushroom was classified as U.

272 Sensitivity and specificity of the classification procedure were computed after the application

273 of the decision tree to all of the mushroom hypercubes.

Results and discussion

RGB images

276 Figure 3 shows representative colour images of the three mushroom classes under

277 investigation in this study. Mushrooms labelled as U (Figure 3a) were white in general

278 appearance, although some of them showed some signs of natural discolouration caused by

279 common picking and transport practice. By day one of storage, MD samples (Figure 3b)

280 exhibited uniform browning over the entire mushroom surface. By day two of storage, *P.*

281 *tolaasii* had colonised the cap of most PT mushrooms (Figure 3c), which exhibited slightly

282 concave brown-coloured spots, the typical symptoms of brown blotch disease.

Confirmation of *P. tolaasii*

284 The prevalence of *Pseudomonas* in mushroom surfaces is high, but only pathogenic *P.*

285 *tolaasii* is capable of causing brown blotch. Two different types of colonies, whose colours

286 were a) creamy and b) green, were found in PAB plates of PT mushrooms, while only one

287 type appeared in PAB plates of U mushrooms and the *P. tolaasii* inoculum; the colour of

288 these colonies was creamy and green, respectively. Isolates of the two types found in PT

289 mushroom plates were obtained by re-streaking representative colonies onto fresh PAB

290 plates. Figure 4 shows growth in PAB plates of the two types of colonies of PT mushrooms

291 (Figures 4a, creamy colonies and 4b, green), the creamy colonies of U mushrooms (Figure

292 4c) and the green colonies of the *P. tolaasii* inoculum (Figure 4d). The creamy colonies of PT

293 mushrooms (Figure 4a) were found to be similar to those found in U plates (Figure 4c), and

294 both gave a negative response to the mushroom tissue block rapid pitting and WLA tests. The

295 green colonies of PT mushrooms (Figure 4b) were similar to those found in *P. tolaasii*

296 inoculum plates (Figure 4d) and both had a positive response to the two pathogenicity tests.

297 These results confirm that the pitting observed in PT mushrooms was due to pathogenic *P.*

298 *tolaasii*.

Spectra

300 Mean spectra of the various spectra classes are shown in Figure 5: (a) non-pretreated

301 reflectance spectra and (b) SNV-corrected reflectance spectra. In Figure 5a, signal intensity

302 and shape differences between U and MD spectra were remarkable. The mean MD spectrum

303 exhibited lower reflectance values over the entire spectral region, as expected after bruising

304 had led to loss of whiteness of the caps. The greatest differences in shape between MD and U

305 spectra arose in the 600-800 nm region, where the mean U spectrum exhibited broader

306 features than the mean MD spectrum. Broad spectra in the visible-near infrared wavelength

307 range are characteristic of undamaged mushrooms, corresponding to their white appearance.

308 The spectral differences mentioned above could be related to the formation of brown

309 pigments, mainly melanins, which derive from enzyme-catalysed oxidation products called

310 quinones. The mean PT spectrum appeared to be more similar in shape to the mean MD

311 spectrum, although its slope was not as linear as MD's was in the 600-800 nm region.

14

312   Spectral differences in Figure 5a arose from differences in sample composition, but

313   differences in illumination conditions, sample height and curvature may also have affected

314   the spectral response of the different mushroom classes. Spectra preprocessing methods such

315   as Multiplicative Scatter Correction (MSC)[38] and SNV[34] can be used to compensate for

316   spectral variability caused by these external factors[39].

317   The mean spectra of SNV-corrected reflectance spectra of U, MD and PT spectra are shown

318   in Figure 5b. Comparing U and MD spectra, MD exhibited higher SNV-corrected reflectance

319   values in the 450-500 nm region and lower SNV-corrected reflectance in the 500-750 nm

320   region. The oxidation of polyphenolic compounds and subsequent development of brown

321   colour in the MD mushrooms might be partly responsible for this dissimilarity[35]. In the 800-

322   950 nm region, MD spectra showed higher values than U mushrooms. Overall, the shape of

323   the mean spectrum of PT spectra was somewhat intermediate between the mean of U and MD

324   spectra in the wavelength range of study. The visible end of the mean PT spectrum looked

325   more similar to MD than to U, whereas its shape in the >700 nm region was very similar to

326   that of U mushrooms'.

327   **PLS-DA analysis**

328   Figure 6 shows RMSECV and performance statistics (i.e. sensitivity and specificity) of the

329   four PLS-DA models developed, as a function of the number of latent variables (from 1 to

330   10). In binary classifications, the sensitivity of a model is a measure of its ability to correctly

331   classify spectra of a given type as being of that type, whereas the specificity is a measure of

332   its ability to correctly classify spectra which are not of a given type as not being of that type.

333   For both U/Dam models (Figs. 6a and 6b), RMSECV exhibited a "corner" (pointed with a red

334   dash circle) at 2 LV. The performance statistics, which were very poor at 1LV, increased at

335   that point and remained at similar levels thereafter, for which 2 was considered to be the

336   optimal # LV for models discriminating between U and Dam spectra. Both MD/PT models

15

337   seemed to perform best when 4 LV were selected; RMSECV did not decrease significantly

338   after that and performance statistics remained high.

339   Numeric values of performance statistics of the selected models are shown in Table 1. When

340   the models built with raw spectra were applied to the training set of spectra, almost perfect

341   classification was achieved in the case of the U/Dam model (sensitivity = 0.997 and

342   specificity = 1.000). The model performed worse when built on SNV-corrected spectra

343   (sensitivity = 0.973 and specificity = 0.999); however differences in sensitivity and

344   specificity were very small. In both cases, almost all of the Dam spectra were classified as

345   such and none or only a few U were misclassified as Dam. When the MD/PT model was

346   applied to the damaged spectra, the sensitivity of the raw model (sensitivity = 0.988) was

347   higher than that of the SNV-corrected model (sensitivity = 0.963), whereas the specificity of

348   the MD/PT_raw model was lower than the MD/PT_SNV model's (0.983 and 0.998,

349   respectively). These results showed that almost all of the spectra of the mushrooms that had

350   been inoculated with *P. tolaasii* were classified correctly and only a few or none of the

351   spectra of the MD samples were misclassified as PT.

352   When the models were applied to the test set of spectra, the sensitivity of the U/Dam_raw

353   model was lower (sensitivity = 0.832) but still none of the U spectra were misclassified as

354   Dam (specificity = 1.000). Performance statistics were quite similar for the U/Dam_SNV

355   model (sensitivity = 0.825 and specificity = 0.999). When the MD/PT model was applied to

356   the damaged spectra of the test set, a smaller percentage of raw PT spectra were classified

357   correctly (sensitivity = 0.661) but almost none of the MD spectra were misclassified as PT

358   (specificity = 0.984). As observed for the previous model, the sensitivity of the MD/PT_SNV

359   model was slightly lower (sensitivity = 0.641) and the specificity was higher (specificity =

360   0.998).

361 Overall, models built on raw reflectance spectra performed better in this study. However,

362 with a view to generalising the use of U/Dam and MD/PT discrimination models, it might be

363 worthwhile to compromise classification performance in favour of employing more versatile

364 models (e.g. models built on SNV-corrected spectra).

Prediction maps

366 Figure 7 shows examples of prediction maps (with no erosion applied in Step 2) of (a) U, (b)

367 MD and (c) PT mushrooms as a result of the application of raw (top row) and SNV-corrected

368 (bottom row) PLS-DA models to the data hypercubes. Overall, predictions by models built on

369 raw reflectance spectra appeared to be more appropriate than predictions by models built on

370 SNV-corrected reflectance spectra: for each mushroom class, the corresponding pixel class

371 was the main pixel class and pixels were distributed in an even manner. In the example

372 shown (Figure 7), on the top row (i.e. predictions by models built on raw reflectance spectra),

373 neither the map of the U mushroom nor the central region of the prediction of the MD

374 mushroom showed misclassification, whereas most edge pixels of the latter were

375 misclassified as U. Considering that all the spectra selected for model building belonged to

376 central regions of the mushrooms, this misclassification could be related to the inability of the

377 models to account for spectral differences due to mushroom surface curvature. Fewer pixels

378 were misclassified in the prediction map of the PT mushroom, where some pixels were

379 classified as MD. On the bottom row of Figure 7 (i.e. prediction maps by models built on

380 SNV-corrected reflectance spectra), the maps of all mushroom types showed

381 misclassification. For U and PT mushrooms, misclassification happened mainly but not only

382 on the edges, where many U pixels were classified as MD. For MD mushrooms, misclassified

383 pixels were distributed evenly along the mushroom surface. In this case, MD pixels were

384 misclassified as PT.

385 Considering that the main focus of this work lies in the identification of PT mushrooms, after

386 visual inspection of the prediction maps (Figure 7), PLS-DA models built on non-pretreated

387 spectra were considered more appropriate for this purpose. Models built on SNV-corrected

388 reflectance spectra were therefore discarded and further sections of this paper will focus only

389 on models built on the raw data.

390 <u>Effect of varying the radius of the SE in Step 2</u>

391 Erosion of a binary image is a basic operation to wear the boundaries of regions away. This

392 can be done to overcome the problem introduced by the so-called "edge effect", by which

393 variability in reflection of light in introduced by spherical surfaces[40]. In this particular case,

394 where PLS-DA models were built on spectra selected from central regions of the mushrooms,

395 it was expected that these models would perform better on central areas of the mushrooms

396 than on edge regions. For this reason, masks defining the mushroom region were eroded

397 using SE's before the models were applied (see Step 2 in *Prediction maps* section). This led

398 to a decrease in misclassified pixels (typically belonging to edge regions, as observed in

399 Figure 7b, top row).

400 Figure 8a shows the effect that increasing the size of the structuring element used in this step

401 (i.e. Step 2) had on the mask (top row) and on the prediction map (bottom row) of a MD class

402 mushroom. As the radius increased (from left to right, from 0 -no erosion- to 40 pixels), the

403 mask became smaller. Consequently, the number of *MD* class pixels that were misclassified

404 (as *U* class) decreased progressively. Figure 8b shows the decrease of the average relative

405 area of the mushroom region as a function of the radius of SE, where the relative area of each

406 mask at a certain SE radius value is displayed as a percentage of the area of the mask when

407 the radius was zero (i.e. when no erosion was applied) and the average and standard deviation

408 values were obtained by considering all the mushrooms in the training and test data sets.

409 Figure 8c shows the sensitivity of the PLS-DA models built on raw reflectance spectra

410   applied at a pixel level as a function of the radius of the SE. The sensitivity of the U/Dam

411   model reached its maximum (sensitivity = 1) at a radius value of 20 pixels when applied to

412   the training set and at a radius value of 40 (sensitivity = 0.972) when applied to the test set.

413   The sensitivity of the MD/PT model was not affected by the radius and remained at its

414   maximum (sensitivity = 1) for the training set, whereas it increased progressively until it

415   reached its maximum (sensitivity = 0.944) at a radius value of 40 pixels. Modifying the

416   radius of the SE did not affect ($p > 0.05$) the specificity of the PLS-DA models (results not

417   shown).

418   <u>Effect of omitting/incorporating Step 4</u>

419   As the existence of isolated *PT* pixels in the prediction map had no physical meaning (brown

420   blotch lesion on mushroom caps are detectable by the human eye), a *closing* step (see Step 4

421   of *Prediction maps* section) was incorporated to the prediction map routine. This step

422   performed dilation followed by erosion on the Bin_{PT} images. Figure 9a shows how the final

423   prediction of a MD class mushroom looked when i) Step 4 was omitted and ii) Step 4 was

424   incorporated in the routine. As it can be observed in the figures, Step 4 removed *PT* class

425   isolated pixels (blue) in the prediction image and converted them into pixels of class *MD*

426   (red). The effect that such conversion had on the performance statistics of the models at a

427   pixel level was studied and only the specificity of the MD/PT_raw model on the test set was

428   found to change significantly ($p < 0.05$). Figure 9b shows how specificity changed as the

429   radius of the SE of Step 2 increased, when i) Step 4 was omitted (round marker) and ii) Step

430   4 was incorporated (square marker) in the routine. The specificity of the MD/PT_raw model

431   improved when this step was incorporated, which means more MD class mushrooms were

432   correctly classified. This figure suggests that adding a *closing* step was important to achieve

433   good levels of classification.

19

434   After studying the two effects, a disk radius of 40 pixels was selected for the SE of Step 2 and

435   it was decided to include Step 4 in the generation of prediction maps. Further sections of this

436   paper will only focus on results based on the use of the aforementioned steps.

437   **Mushroom classification**

438   The application of PLS-DA models built on raw spectra to the totality of entire hypercubes

439   led to the performance statistics shown in Table 2. For the training set mushrooms, both the

440   sensitivity and the specificity of the U/Dam_raw model were 1, which means there was no

441   misclassification at all. For the same samples, the sensitivity of the MD/PT_raw model was 1

442   and its specificity was 0.98. Only 1 out of 48 MD mushroom was misclassified as a PT

443   mushroom. The models performed quite similarly for the mushroom hypercubes of the test

444   set: for the U/Dam_raw model, sensitivity = 0.97 and specificity = 1. Only 2 out of 72 Dam

445   mushrooms were misclassified as U, and none of the U was misclassified as Dam. For the

446   MD/PT_raw model, sensitivity = 0.944 (only 2 out of 36 PT mushrooms were not classified

447   as such) and specificity = 0.97 (only 1 MD mushroom was misclassified as being PT).

448   These results show the models performed well when applied at a pixel level and could be the

449   first step towards the development of a HSI sensor that would classify independent sets of

450   mushrooms with high levels of accuracy. Overall, the correct classification of the models

451   presented in this paper is higher than the classification of the algorithms by Vízhányó and

452   Felföldi[9], which correctly classified 81% of the diseased areas of test mushrooms using

453   conventional computer imaging. It should be noted that the procedure described in this paper

454   is longer and more complex than the one presented in that study, and the technology more

455   costly. While the algorithms presented in the aforementioned paper discriminated diseased

456   spots from healthy senescent mushroom parts, the models developed in this paper

457   discriminate microbial spoilage from both undamaged and mechanically damaged samples.

458 The correct discrimination between PT and MD mushrooms ensure no misclassification of

459 samples whose colour analysis might be similar and hence avoid "false positives".

Conclusion

461 Results presented in this work show that raw reflectance data of mushroom caps could be

462 used to classify mushrooms according to their damage class (i.e. undamaged, mechanically

463 damaged or brown blotch diseased). PLS-DA models were developed to initially sort

464 mushrooms into undamaged or damaged classes and to further classify the damaged into

465 mechanically damaged or microbiologically diseased classes. The application of the models

466 at a pixel level together with the use of a decision tree allowed for correct classification of

467 >95%. This study demonstrates the potential use of hyperspectral imaging as an automated

468 tool for detection of brown blotched mushrooms and for their discrimination from

469 mechanically damaged mushrooms. Knowledge gained in this research using HSI could be

470 incorporated towards the development of simpler sensors to detect and classify mushroom

471 damage of different sources. Such a system could aid the industry in increasing quality

472 control standards by correctly identifying low quality produce. However, further research and

473 validation at industrial scale are required to facilitate its adoption.

References

482 1. S.G. Paine, "Studies in Bactoeriosis II: A Brown Blotch Disease of Cultivated

483   Mushrooms", *Annals of Applied Biology* **5,** [1919].

484 2. N.G. Nair and J.K. Bradley, "Mushroom Blotch Bacterium During Cultivation", *The*

485   *Mushroom Journal* **90,** [1980].

486 3. C. Soler-Rivas, S. Jolivet, N. Arpin, J.M. Olivier and H.J. Wichers, "Biochemical and

487   Physiological Aspects of Brown Blotch Disease of *Agaricus Bisporus*", *FEMS*

488   *Microbiology Reviews* **23,** [1999].

489 4. P.B. Rainey, C.L. Brodey and K. Johnstone, "Biology of *Pseudomonas Tolaasii*,

490   Cause of Brown Blotch Disease of the Cultivated Mushrooms", in *Advances in Plant*

491   *Pathology* **8**, Ed by J.H. Andrews and I.C. Tommerup. Academic Press, p. 95-117

492   [1992].

493 5. F. Moquet, M. Mamoun and J.M. Olivier, "*Pseudomonas Tolaasii* and Tolaasin:

494   Comparison of Symptom Induction on a Wide Range of *Agaricus Bisporus* Strains",

495   *FEMS Microbiology Letters* **142,** [1996].

496 6. J.C. Nutkins, R.J. Mortishire-Smith, L.C. Packman, C.L. Brodey, P.B. Rainey, K.

497   Johnstone and D.H. Williams, "Structure Determination of Tolaasin, an Extracellular

498   Lipodepsipeptide Produced by Mushroom Pathogen *Pesudomonas Tolaasii* Paine",

499   *Journal of American Chemical Society* **113,** [1991].

500 7. J.M. Olivier, J. Guillaumes and D. Martin, "Study of a Bacterial Disease of

501   Mushroom Caps", in *4th International Conference on Plant Pathogenic Bacteria*,

502   Angers, France [1978].

503 8. P.H. Heinemann, R. Hughes, C.T. Morrow, H.J. Sommer, R.B. Beelman and P.J.

504   Wuest, "Grading of Mushrooms Using a Machine Vision System", *Transactions of*

505   *the ASAE* **37,** 5 [1994].

506   9.   T. Vízhányó and J. Felföldi, "Enhancing Colour Differences in Images of Diseased
507   Mushrooms", *Computers and Electronics in Agriculture* **26,** [2000].

508   10.   S. Jolivet, N. Arpin, H.J. Wichers and G. Pellom, "*Agaricus Bisporus* Browning: A
509   Review", *Mycological Research* **102,** 12 [1998].

510   11.   A.A. Gowen, C.P. O'Donnell, P.J. Cullen, G. Downey and J.M. Frías, "Hyperspectral
511   Imaging - an Emerging Process Analytical Tool for Food Quality and Safety Control",
512   *Trends in Food Science and Technology* **18,** [2007].

513   12.   A.A. Gowen, C.P. O'Donnell, M. Taghizadeh, P.J. Cullen, J.M. Frias and G. Downey,
514   "Characterisation of Blemishes on White Mushroom (*Agaricus Bisporus*) Caps Using
515   Hyperspectral Imaging", in *10th International conference on Engineering and Food -*
516   *ICEF 10*, Viña del Mar, Chile [2008].

517   13.   Y. Peng and R. Lu, "Analysis of Spatially Resolved Hyperspectral Scattering Images
518   for Assessing Apple Fruit Firmness and Soluble Solids Content", *Postharvest Biology*
519   *and Technology* **48,** 1 [2008].

520   14.   S.T. Monteiro, Y. Minekawa, Y. Kosugi, T. Akazawa and K. Oda, "Prediction of
521   Sweetness and Amino Acid Content in Soybean Crops from Hyperspectral Imagery",
522   *ISPRS Journal of Photogrammetry and Remote Sensing* **62,** 1 [2007].

523   15.   J. Qiao, N. Wang, M. Ngadi and S. Baljinder, "Water Content and Weight Estimation
524   for Potatoes Using Hyperspectral Imaging", in *2005 ASAE Annual Meeting, Paper*
525   *No. 053126*, St. Joseph, Michigan, USA [2005].

526   16.   L. Liu, M.O. Ngadi, S.O. Prasher and C. Gariépy, "Categorization of Pork Quality
527   Using Gabor Filter-Based Hyperspectral Imaging Technology", *Journal of Food*
528   *Engineering* **99,** 3 [2010].

529   17.   H.K. Noh and R. Lu, "Hyperspectral Laser-Induced Fluorescence Imaging for
530   Assessing Apple Fruit Quality", *Postharvest Biology and Technology* **43,** 2 [2007].

531   18.   B. Park, K.C. Lawrence, W.R. Windham and D.P. Smith, "Performance of

532   Hyperspectral Imaging System for Poultry Surface Fecal Contaminant Detection",

533   *Journal of Food Engineering* **75,** 3 [2006].

534   19.   Y. Liu, Y.-R. Chen, M.S. Kim, D.E. Chan and A.M. Lefcourt, "Development of

535   Simple Algorithms for the Detection of Fecal Contaminants on Apples from

536   Visible/near Infrared Hyperspectral Reflectance Imaging", *Journal of Food*

537   *Engineering* **81,** 2 [2007].

538   20.   D.P. Ariana and R. Lu, "Evaluation of Internal Defect and Surface Color of Whole

539   Pickles Using Hyperspectral Imaging", *Journal of Food Engineering* **96,** 4 [2010].

540   21.   J. Dubois, E. Neil Lewis, J.F.S. Fry and E.M. Calvey, "Bacterial Identification by

541   near-Infrared Chemical Imaging of Food-Specific Cards", *Food Microbiology* **22,** 6

542   [2005].

543   22.   M.F. Escoriza, J.M. VanBriesen, S. Stewart, J. Maier and P.J. Treado, "Raman

544   Spectroscopy and Chemical Imaging for Quantification of Filtered Waterborne

545   Bacteria", *Journal of Microbiological Methods* **66,** 1 [2006].

546   23.   A.A. Gowen, C.P. O'Donnell, M. Taghizadeh, P.J. Cullen and G. Downey,

547   "Hyperspectral Imaging Combined with Principal Component Analysis for Bruise

548   Damage Detection on White Mushrooms (*Agaricus Bisporus*)", *Journal of*

549   *Chemometrics* **22,** 3-4 [2008].

550   24.   A.A. Gowen, M. Taghizadeh and C.P. O'Donnell, "Identification of Mushrooms

551   Subjected to Freeze Damage Using Hyperspectral Imaging", *Journal of Food*

552   *Engineering* **93,** 1 [2009].

553   25.   M. Taghizadeh, A. Gowen and C.P. O'Donnell, "Prediction of White Button

554   Mushroom (*Agaricus Bisporus*) Moisture Content Using Hyperspectral Imaging",

555   *Sensing and Instrumentation for Food Quality and Safety* **4,** [2009].
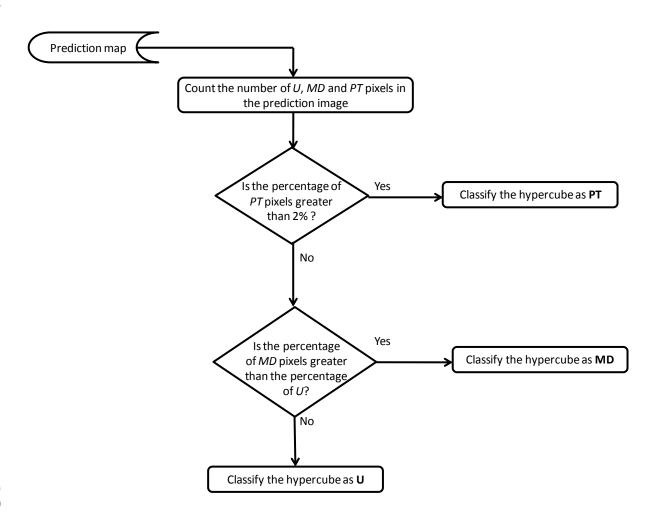
556 26. E. Gaston, J.M. Frías, P.J. Cullen, C.P. O'Donnell and A.A. Gowen, "Prediction of
557 Polyphenol Oxidase Activity Using Visible near-Infrared Hyperspectral Imaging on
558 Mushroom (*Agaricus Bisporus*) Caps*", Journal of Agricultural and Food Chemistry,*
559 doi: 10.1021/jf00501q.

560 27. M. Taghizadeh, A. Gowen and C.P. O'Donnell, "Use of Hyperspectral Imaging for
561 Evaluation of the Shelf-Life of Fresh White Button Mushrooms (*Agaricus Bisporus*)
562 Stored in Different Packaging Films*", Innovative Food Science and Emerging*
563 *Technologies,* doi: 10.1016/j.ifset.2010.01.016.

564 28. A.A. Gowen, C.P. O'Donnell, M. Taghizadeh, E. Gaston, A. O'Gorman, P.J. Cullen,
565 J.M. Frías, C. Esquerre and G. Downey, "Hyperspectral Imaging for the Investigation
566 of Quality Deterioration in Sliced Mushrooms (*Agaricus Bisporus*) During Storage",
567 *Sensing and Instrumentation for Food Quality and Safety* **2,** 3 [2008].

568 29. D.P. Ariana, R. Lu and D.E. Guyer, "Near-Infrared Hyperspectral Reflectance
569 Imaging for Detection of Bruises on Pickling Cucumbers", *Computers and*
570 *Electronics in Agriculture* **53,** 1 [2006].

571 30. B.M. Nicolaï, E. Lötze, A. Peirs, N. Scheerlinck and K.I. Theron, "Non-Destructive
572 Measurement of Bitter Pit in Apple Fruit Using Nir Hyperspectral Imaging",
573 *Postharvest Biology and Technology* **40,** 1 [2006].

574 31. G. ElMasry, N. Wang and C. Vigneault, "Detecting Chilling Injury in Red Delicious
575 Apple Using Hyperspectral Imaging and Neural Networks", *Postharvest Biology and*
576 *Technology* **52,** 1 [2009].

577 32. J. Gómez-Sanchis, L. Gómez-Chova, N. Aleixos, G. Camps-Valls, C. Montesinos-
578 Herrero, E. Moltó and J. Blasco, "Hyperspectral System for Early Detection of
579 Rottenness Caused by Penicillium Digitatum in Mandarins", *Journal of Food*
580 *Engineering* **89,** 1 [2008].

581   33.   W.C. Wong and T.F. Preece, "Identification of *Pseudomonas Tolaasii* : The White

582   Line in Agar and Mushroom Tissue Block Rapid Pitting Tests", *Journal of Applied*

583   *Bacteriology* **47,** [1979].

584   34.   R.J. Barnes, M.S. Dhanoa and S.J. Lister, "Standard Normal Variate Transformation

585   and Detrending of near Infrared Diffuse Reflectance Spectroscopy", *Applied*

586   *Spectroscopy* **43,** 5 [1989].

587   35.   C. Esquerre, A.A. Gowen, C.P. O'Donnell and G. Downey, "Initial Studies on the

588   Quantitation of Bruise Damage and Freshness in Mushrooms Using Visible-near-

589   Infrared Spectroscopy", *Journal of Agricultural and Food Chemistry* **57,** [2009].

590   36.   R_Development_Core_Team, *R: A Language and Environment for Statistical*

591   *Computing*. R Foundation for Statistical Computing, Vienna, Austria [2007].

592   37.   A. Rocha, D.C. Hauagge, J. Wainer and S. Goldenstein, "Automatic Fruit and

593   Vegetable Classification from Images", *Computers and Electronics in Agriculture* **70,**

594   1 [2010].

595   38.   P. Geladi, D. MacDougall and H. Martens, "Linearization and Scatter-Correction for

596   near-Infrared Reflectance Spectra of Meat", *Applied Spectroscopy* **39,** 3 [1985].

597   39.   T. Azzouz, A. Puigdoménech, M. Aragay and R. Tauler, "Comparison between

598   Different Data Pre-Treatment Methods in the Analysis of Forage Samples Using near-

599   Infrared Diffuse Reflectance Spectroscopy and Partial Least-Squares Multivariate

600   Calibration Method", *Analytica Chimica Acta* **484,** [2003].

601   40.   J. Blasco, N. Aleixos and E. Moltó, "Machine Vision System for Automatic Quality

602   Grading of Fruit", *Biosystems Engineering* **85,** 4 [2003].

603

604

605

Visible Near-Infrared Hyperspectral Imaging for the Identification and Discrimination of Brown Blotch Disease on Mushroom (*Agaricus bisporus*) Caps.

E. Gaston, Jesús M. Frías, Patrick J. Cullen, Colm P. O'Donnell and Aoife A. Gowen
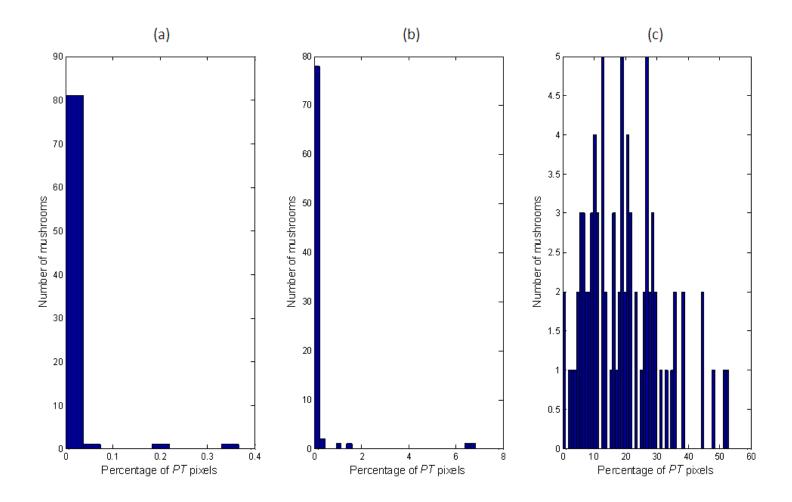
606 **Figures**

607 **Figure 1**

608

611 **Figure 1** Decision tree for mushroom hypercube classification, where U = undamaged, MD =
612 mechanically damaged and PT = P. tolaasii inoculated.

613

614

Figure 2 Histograms showing number of mushrooms as a function of the percentage of pixels in the BIN_{PT} binary images of (a) undamaged (U), (b) mechanically damaged (MD) and (c) P.tolaasii inoculated (PT) mushrooms. All the mushrooms (i.e. training and test set mushrooms) of each class were plotted together, making a total of 86 samples per mushroom class.

Visible Near-Infrared Hyperspectral Imaging for the Identification and Discrimination of Brown Blotch Disease on Mushroom (*Agaricus bisporus*) Caps.

E. Gaston, Jesús M. Frías, Patrick J. Cullen, Colm P. O'Donnell and Aoife A. Gowen
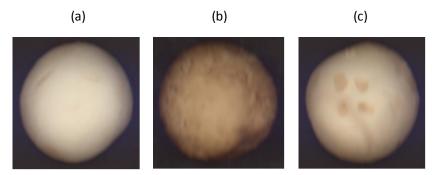
619 **Figure 3**

620

(a) (b) (c)

621

622 **Figure 3** Representative colour images of (a) undamaged (U), (b) mechanically damaged
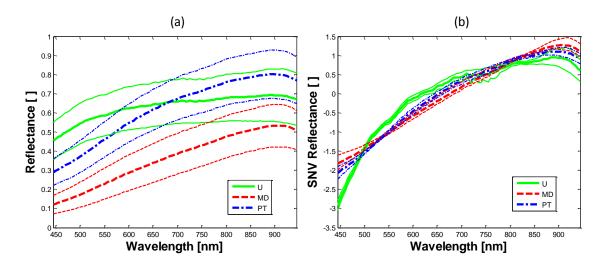623 (MD) and (c) *P. tolaasii* inoculated (PT) mushrooms.

624 **Figure 4**

625

626

627 **Figure 4** (a) Creamy colonies in PAB plate of PT mushrooms, (b) Green colonies in PAB
628 plate of PT mushrooms, (c) Creamy colonies in PAB plate of U mushrooms and (d) Green
629 colonies in PAB plate of *P.tolaasii* inoculum.

630 **Figure 5**

631

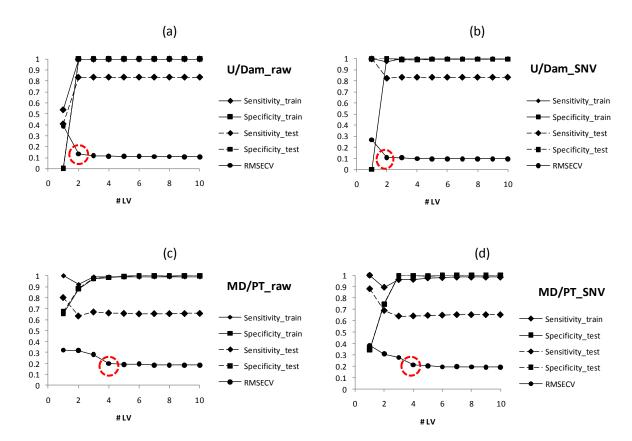632 **Figure 5** (a) Mean ± standard deviation raw reflectance spectra and (b) mean ± standard
633 deviation SNV-corrected reflectance spectra of selected regions of undamaged (U),
634 mechanically damaged (MD) and *P. tolaasii* inoculated (PT) mushroom caps. For each
635 mushroom group, the broader line represents mean spectrum and the narrower lines represent
636 ± standard deviation spectra.

637

Visible Near-Infrared Hyperspectral Imaging for the Identification and Discrimination of Brown Blotch Disease on Mushroom (*Agaricus bisporus*) Caps.

E. Gaston, Jesús M. Frías, Patrick J. Cullen, Colm P. O'Donnell and Aoife A. Gowen
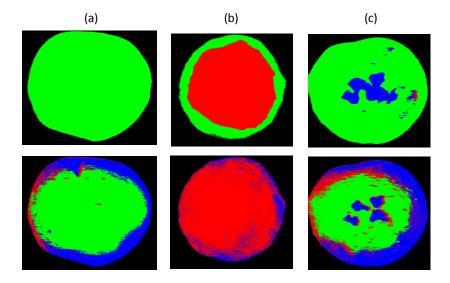
638 **Figure 6**

639

640 **Figure 6** Root-mean square error of cross-validation (RMSECV) and performance statistics
641 (i.e. sensitivity and specificity) of PLS-DA models of (a) U/Dam_raw model, (b)
642 U/Dam_SNV model, (c) MD/PT_raw model and (d) MD/PT_SNV model as a function of the
643 number of latent variables (# LV), where _train = training set and _test = test set.

Visible Near-Infrared Hyperspectral Imaging for the Identification and Discrimination of Brown Blotch Disease on Mushroom (*Agaricus bisporus*) Caps.

E. Gaston, Jesús M. Frías, Patrick J. Cullen, Colm P. O'Donnell and Aoife A. Gowen

644 **Figure 7**

645

646

647 **Figure 7** Prediction images (after no erosion in Step 2) of (a) undamaged (U), (b)
648 mechanically damaged (MD) and (c) *P. tolaasii* inoculated (PT) mushrooms by PLS-DA
649 models built on raw reflectance spectra (top row) and SNV-corrected reflectance spectra
650 (bottom row).

Visible Near-Infrared Hyperspectral Imaging for the Identification and Discrimination of Brown Blotch Disease on Mushroom (*Agaricus bisporus*) Caps.

E. Gaston, Jesús M. Frías, Patrick J. Cullen, Colm P. O'Donnell and Aoife A. Gowen

651   **Figure 8**

(a)

no erosion   disk radius = 10 pixels   disk radius = 20 pixels   disk radius = 30 pixels   disk radius = 40 pixels

(b)   (c)
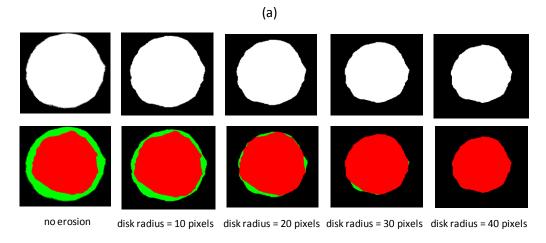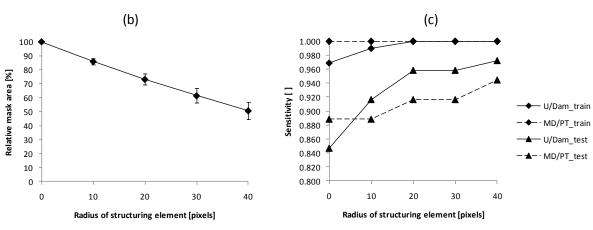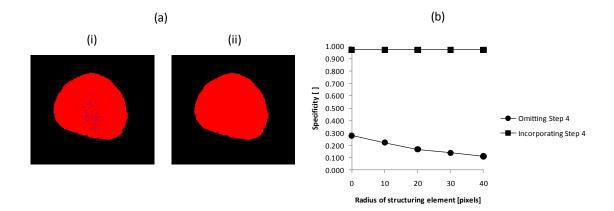
652

653   **Figure 8** (a) Binary masks (top row) and prediction maps (bottom row) of a mechanically
654   damaged (MD) mushroom, (b) Average relative mask area ± SD and (c) Sensitivity of PLS-
655   DA models, as a function of the radius of the structuring element (SE) used for erosion in
656   Step 2.

Visible Near-Infrared Hyperspectral Imaging for the Identification and Discrimination of Brown Blotch Disease on Mushroom (*Agaricus bisporus*) Caps.

E. Gaston, Jesús M. Frías, Patrick J. Cullen, Colm P. O'Donnell and Aoife A. Gowen

657 **Figure 9**

658

659

660 **Figure 9** Effect of the exclusion/incorporation of Step 4 to the prediction map routine in
661 terms of (a) the pixel distribution in the prediction map of a mechanically damaged (MD)
662 mushroom when (i) Step 4 was omitted and (ii) Step 4 was incorporated and (b) the
663 Specificity of the MD/PT_raw model on the test set as a function of the radius of the
664 structuring element (SE) used for erosion in Step 2.

665 .

Visible Near-Infrared Hyperspectral Imaging for the Identification and Discrimination of Brown Blotch Disease on Mushroom (*Agaricus bisporus*) Caps.

E. Gaston, Jesús M. Frías, Patrick J. Cullen, Colm P. O'Donnell and Aoife A. Gowen

666 # Tables

667 **Table 1**

668 **Table 1** Performance statistics at spectra level of all the PLS-DA models built on reflectance
669 spectra.

Model	# LV	TRAINING SET		TEST SET	
		Sensitivity	Specificity	Sensitivity	Specificity
U/Dam_raw	2	0.997	1	0.832	1
U/Dam_SNV	2	0.973	0.999	0.825	0.999
MD/PT_raw	4	0.988	0.983	0.661	0.984
MD/PT_SNV	4	0.963	0.998	0.641	0.998

670

Visible Near-Infrared Hyperspectral Imaging for the Identification and Discrimination of Brown Blotch Disease on Mushroom (*Agaricus bisporus*) Caps.

E. Gaston, Jesús M. Frías, Patrick J. Cullen, Colm P. O'Donnell and Aoife A. Gowen

671   **Table 2**

672   **Table 2** Performance statistics at a pixel level PLS-DA models built on raw reflectance
673   spectra.

Model	TRAINING SET		TEST SET	
	Sensitivity	Specificity	Sensitivity	Specificity
U/Dam_raw	1	1	0.972	1
MD/PT_raw	1	0.979	0.944	0.972

674